The Abdus Salam
International Centre for Theoretical Physics

United Nations
Educational, Scientific
and Cultural Organization

International Atomic
Energy Agency

SMR 1673/35

AUTUMN COLLEGE ON PLASMA PHYSICS

5 - 30 September 2005

High frequency waves in electron foreshock region: Cluster results". Part II

Vladimir Krasnoselskikh
LPCE / CNRS-University of Orleans
France

"High frequency waves in electron foreshock region: Cluster results". Part II.

V. Krasnoselskikh (LPCE, France)

with the assistance of

V. Lobzin, B. Lefebvre, S. Schwartz, I. H. Cairns, P. Décréau, J. Soucek, T. Dudok de Wit, J. Pickett, C. Kletzing

Outline

- Properties of high frequency plasma waves in the electron foreshock observed the WBD instrument of CLUSTER:
  - Multiple Langmuir wave peaks
  - PDF of waves ampltudes
  - Relationship between wave amplitude and the characteristic time of its modulation.

- Interpretation of experimental results in terms of parametric decay instability and filamentation of Langmuir waves

The foreshock

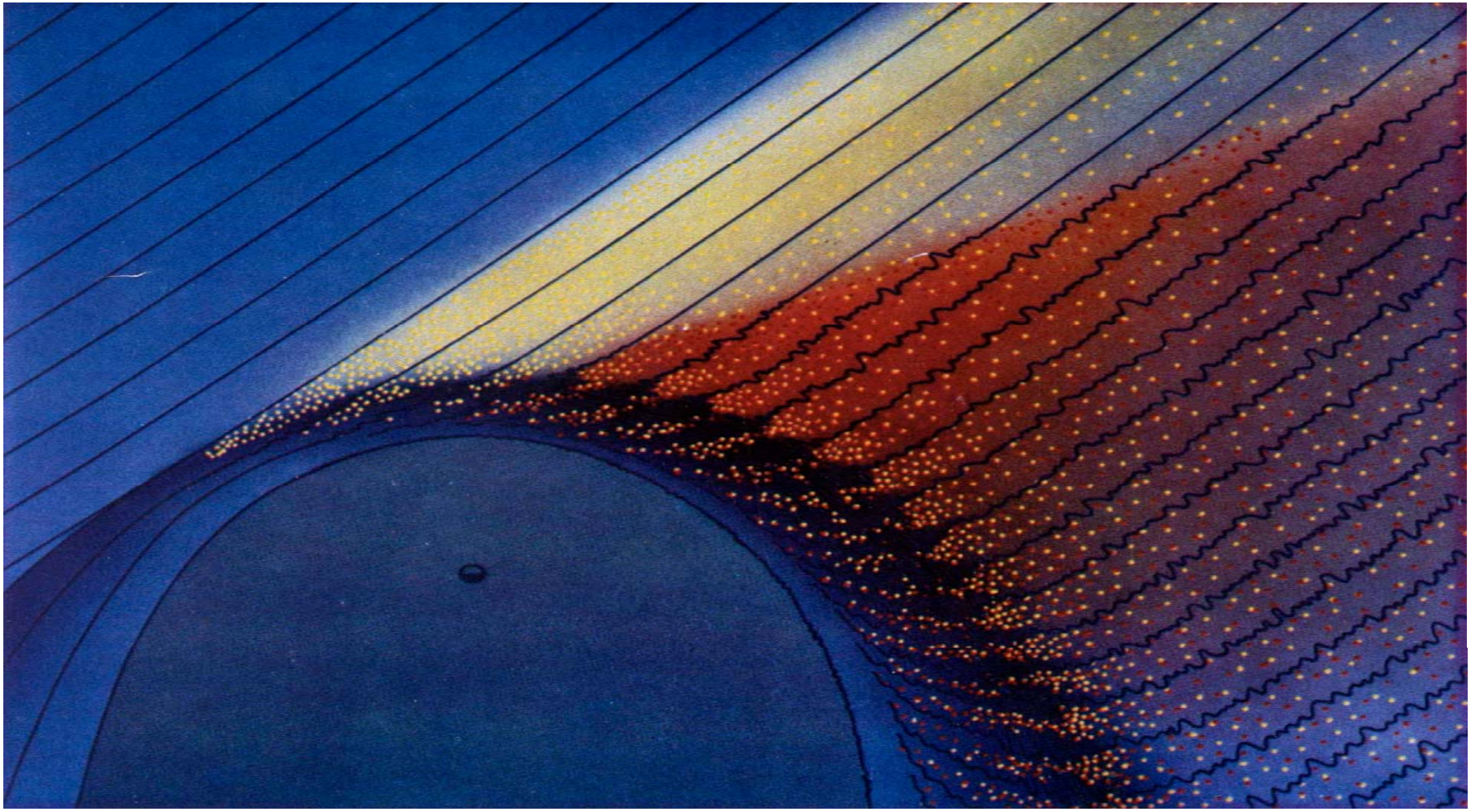

JOURNAL OF GEOPHYSICAL RESEARCH, VOL. 110, A08102, doi:10.1029/2004JA010977, 2005

Nonlinear decay of foreshock Langmuir waves in the presence of plasma inhomogeneities: Theory and Cluster observations

J. Soucek,[1,2] V. Krasnoselskikh,[1] T. Dudok de Wit,[1] J. Pickett,[3] and C. Kletzing[3]

Received 14 December 2004; revised 14 April 2005; accepted 21 April 2005; published 11 August 2005.

[1] The intense high-frequency electrostatic waves observed in the terrestrial foreshock often have a form of a superposition of two monochromatic waves close to the plasma frequency. We suggest an interpretation of these spectra as signatures of nonlinear decay of Langmuir waves to electron-sound and ion-sound secondary waves. This decay instability is known to have different properties in inhomogeneous plasma, namely the threshold amplitude of this instability is inversely proportional to the scale of the inhomogeneity. We show that the observed dependence of the wave amplitude on the modulation scale of the wave packets is consistent with this property and the theory of absolute decay instability in inhomogeneous plasma can be applied to explain the satellite observations. In this study we used electric field data from the Wide Band Data instrument on board Cluster satellites.

Experimental data overview

- High frequency electric field data from the WBD instrument of CLUSTER
- Measures one component of the E-field
- Band-pass filtered between 1 kHz and 77 kHz
- WBD operates in duty cycles - each block of data is 10 milliseconds long and is followed by a gap of 80ms. The size of this block imposes limits the spectral resolution of the Fourier transform.

Typical waveforms

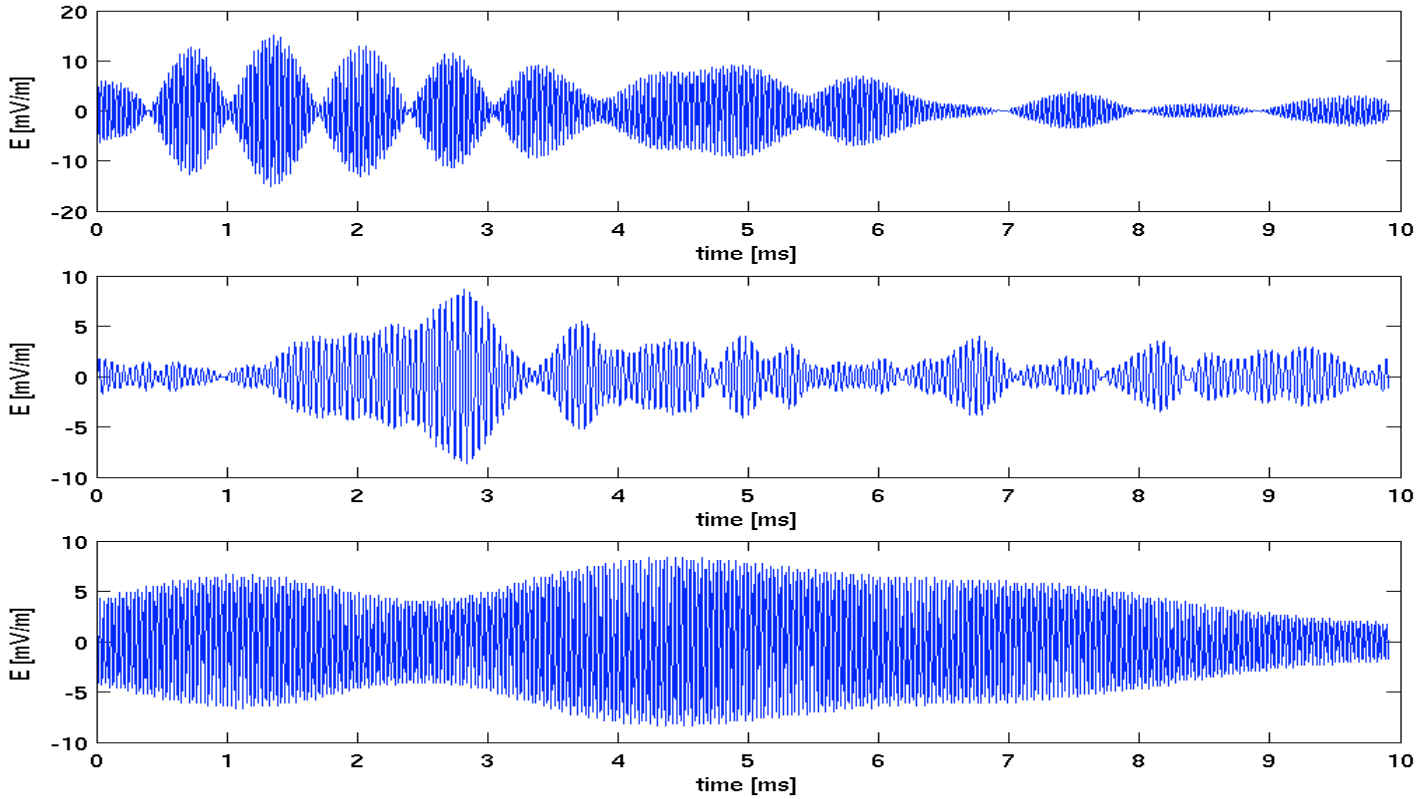

Electric field waveforms observed in the foreshock usually have the form of a slowly modulated monochromatic wave. The modulation often shows a signature of interference of 2 or more waves.

Double/Triple peaked spectra

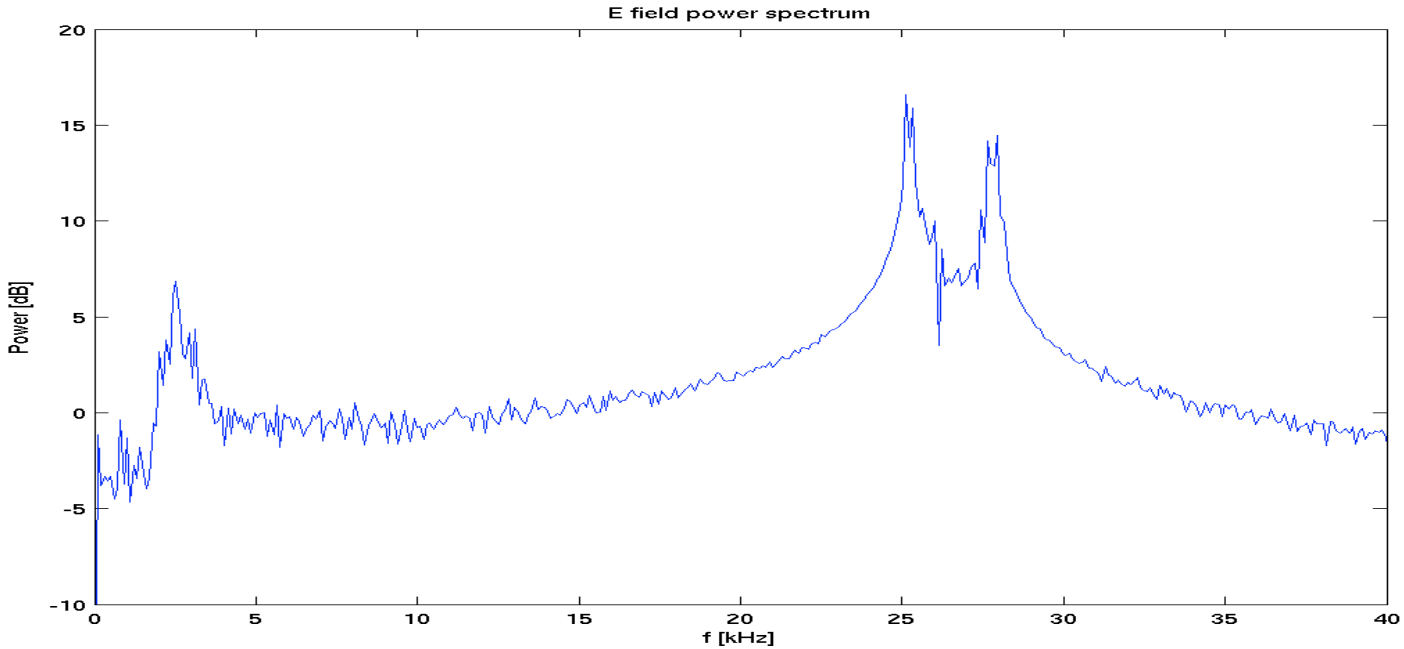

- Corresponding spectra often show two Langmuir peaks of comparable amplitude and sometimes (if instrumental constraints allow) a weaker low frequency wave.
- The frequencies of this triplet often satisfy the resonance condition $f_{LF} = f_{HF1} + f_{HF2}$

Non-linear wave decay

- Nonlinear parametric decay is frequently proposed as the mechanism saturating growth of beam-generated large amplitude Langmuir waves in the solar wind.
- Once the wave amplitude exceeds certain threshold value, parametric instability sets in and a Langmuir wave decays into two secondary waves transferring its energy to the product waves. The secondary waves must satisfy resonance conditions for frequencies and wawe-number:

$$k_0 = k_1 + k_2$$
$$\omega_0 = \omega_1 + \omega_2$$

- In the solar wind, where plasma is composed of two electron populations (hot and cold), the decay can proceed in two chanels:

Langmuir wave (ω_0) $\rightarrow$ Langmuir (ω_1) + ion-sound (ω_2) waves

Langmuir wave (ω_0) $\rightarrow$ electron-sound (ω_1) + ion-sound (ω_2) waves

Non-linear wave decay (basic theory)

- One Langmuir wave decays into another Langmuir (or electron-sound) wave and an ion-sound wave. ($L \rightarrow L' + S$)
- Frequencies and wavenumbers must satisfy resonance conditions

$$k(L) = k(L') + k(S)$$
$$\omega(L) = \omega(L') + \omega(S)$$

- The product ion-acoustic wave in general much weak than the parent high-frequency wave
- This nonlinear process can proceed only if the wave amplitude exceeds certain threshold. Amplitudes of foreshock waves (~ 1-10 mV/m) are comparable with the threshold estimated from t6ypical observed plasma parameters [Robinson et al,. GRL, 1995].
- Phases of the waves should be coupled:

$$\Phi(L) - \Phi(L') - \Phi(S) = \text{const.}$$

Doppler shift

- From the magnitude of the Doppler shift ($\Delta f \approx 3$ kHz) we can conclude, that the secondary wave cannot be a Langmuir wave. For observed plasma parameters and solar wind speed of 450 km/s, the maximum possible Doppler shift would be approximately 750 Hz, which is significantly less than what is observed.

- Electron sound waves have larger k-vectors and allow for much larger frequency Doppler shifts. From that we conclude, that the secondary wave is most likely an electron-sound wave.

The Event (March 16, 2001)

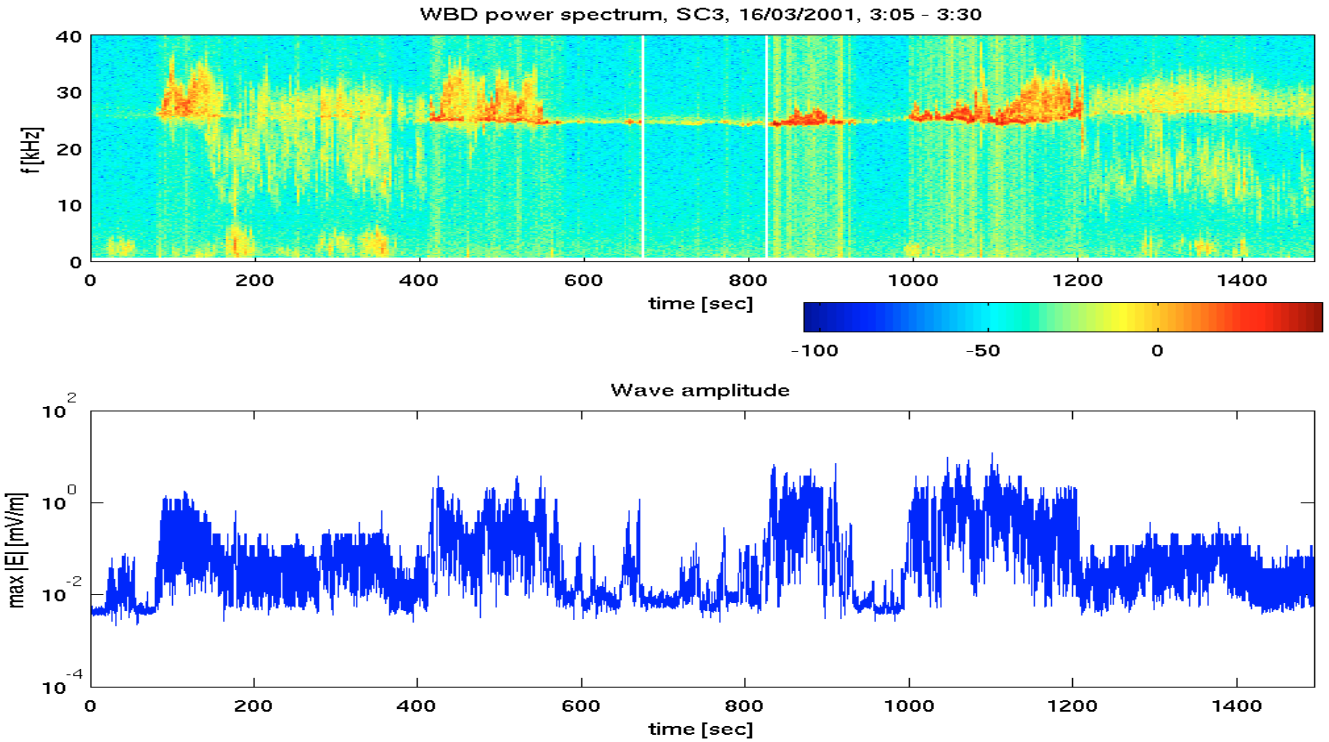

- CLUSTER in the Earth‘s foreshock
  (Diff = 0 .. - 6 R_E)
- Observed wave amplitudes up to 5 mV/m

Spectrum in detail

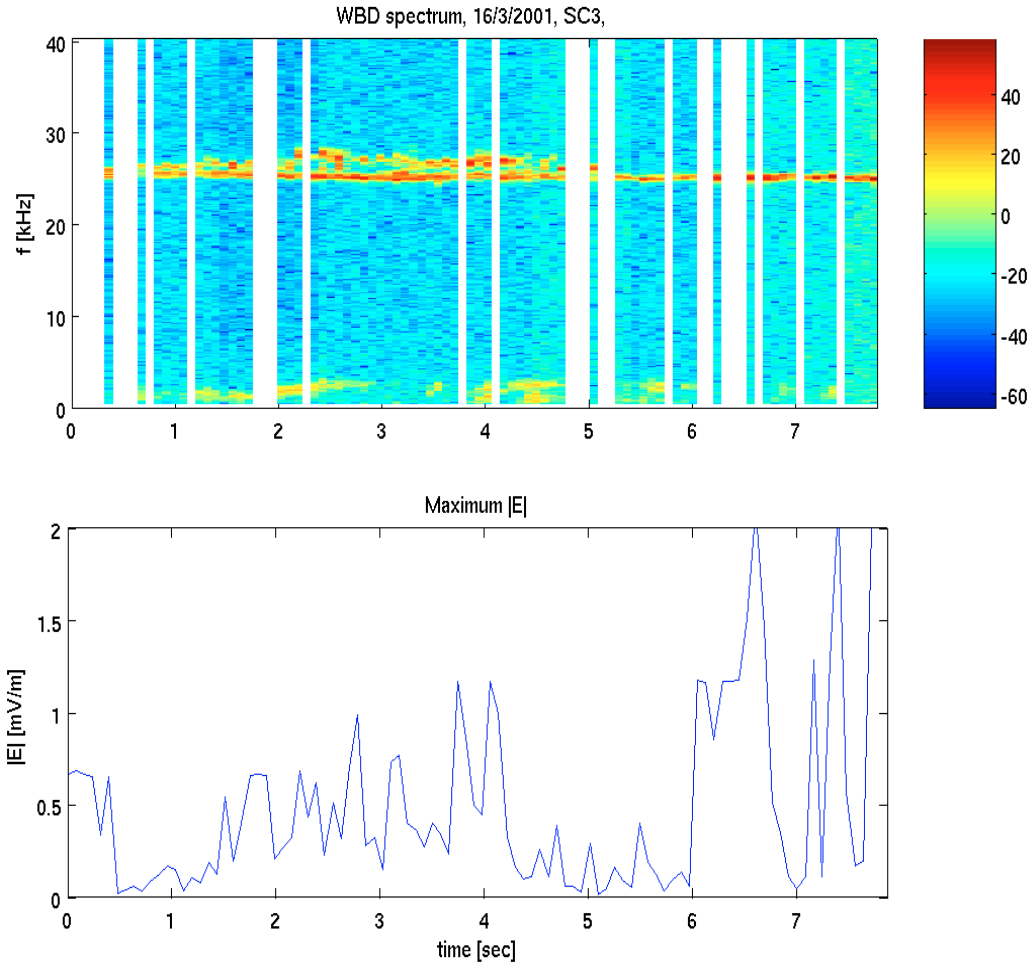

This detailed spectrogram shows how the resonance condition between the wave frequencies is conserved. The frequency of the low frequency wave follows agrees with the frequency difference of the two high-frequency peaks even if this difference changes with time.

In further analysis, we will prove this statement statistically.

Technique for automatic verification of resonance condition of the frequencies $f_0 = f_1 + f_2$

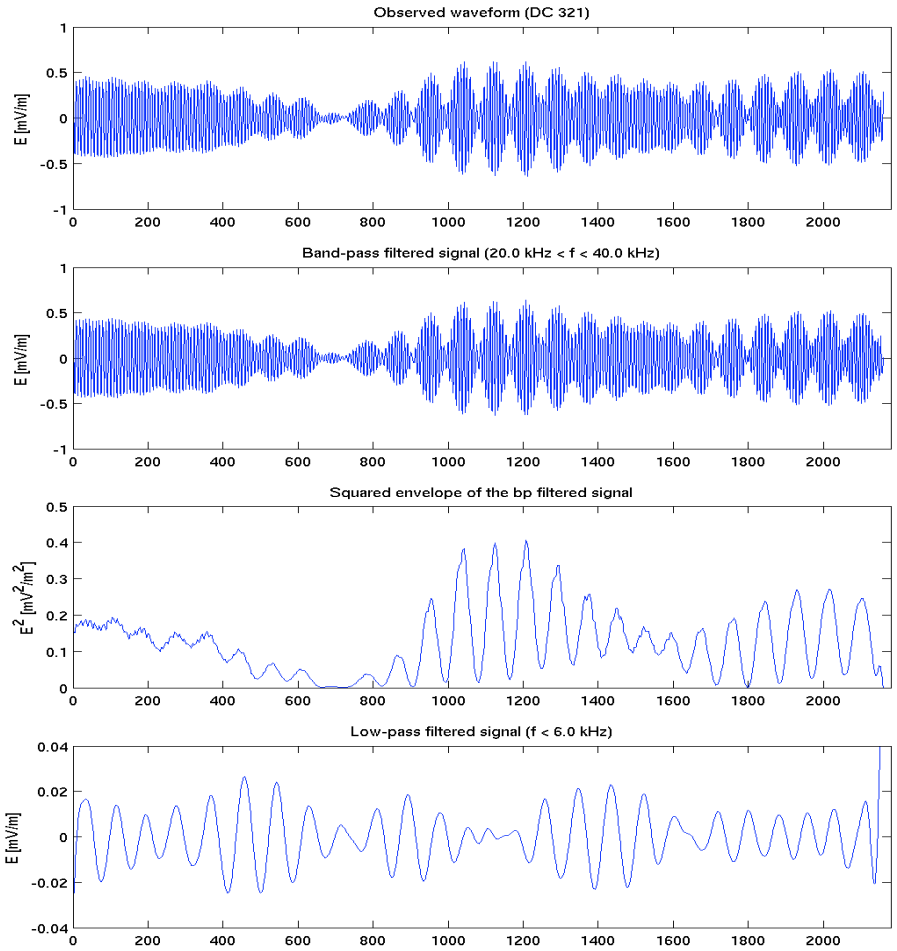

Observed waveform

Filtered waveform, only HF kept

Envelope of HF wave

Low-pass filtered waveform

Statistical ensemble

Now we apply this technique to a large ensemble of observed waveforms with amplitudes above 0.1 mV/m. We only select waveforms which contain some above threshold low frequency component and which are properly represented within the 8-bit digitization range of the instrument.

We compare the peak frequency of the low-pass filtered waveform and the frequency of the envelope modulation, equal to the frequency difference of the primary Langmuir and secondary electron sound wave.

Statistics of the frequencies

Joint distribution of wave-beating frequencies versus the corresponding ion-sound wave frequencies (3654 samples)

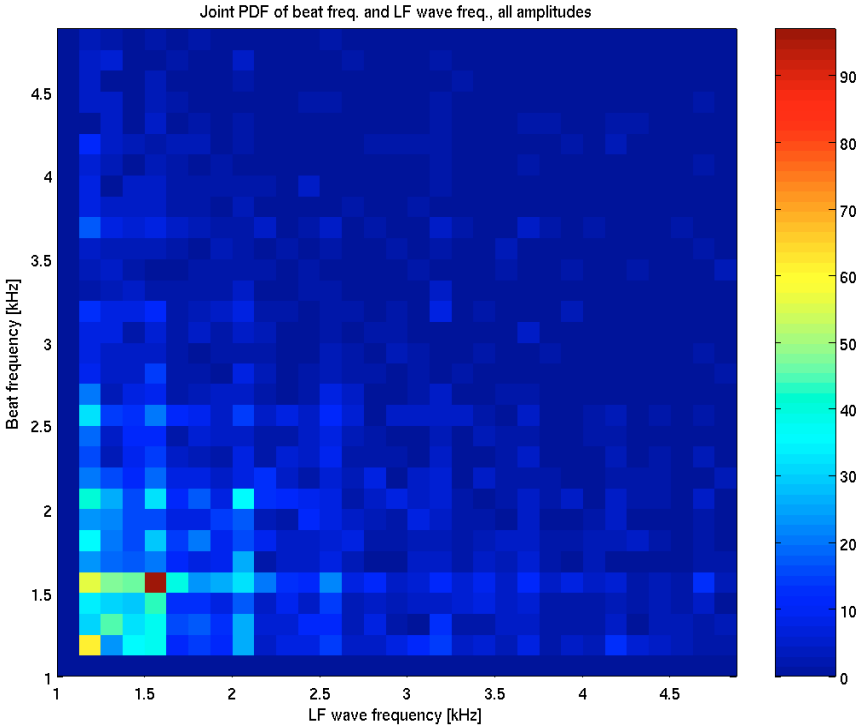

Same histogram, but now only events with amplitude higher than 0.5 mV/m vere included. (228 samples)

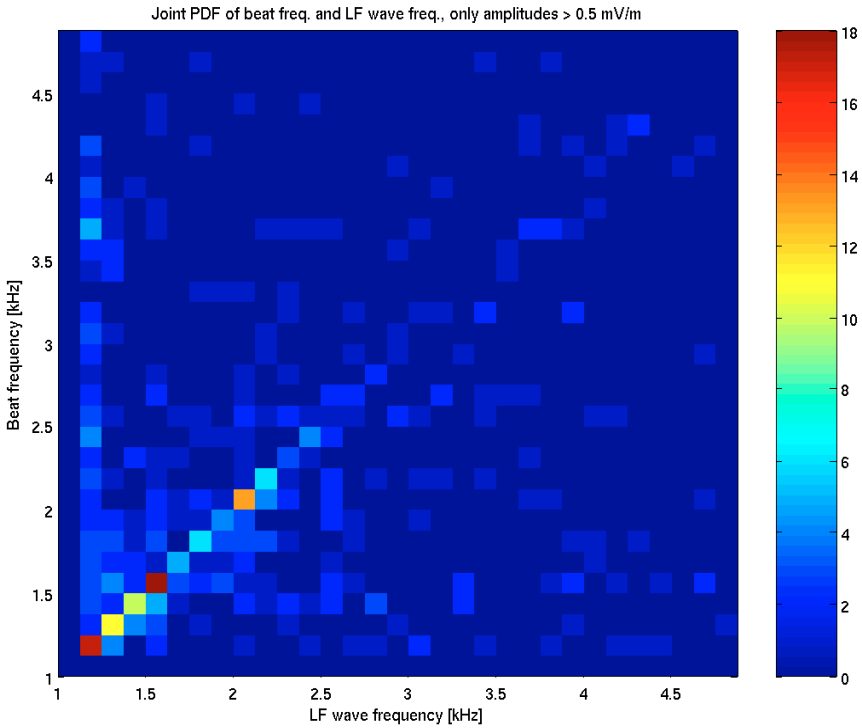

The above plots show that the resonance condition for frequencies of the triplets is more likely to be satisified for the waves of higher amplitude.

Statistics of the phases

Histogram of cross-phases between Langmuir wave envelope and LF wave

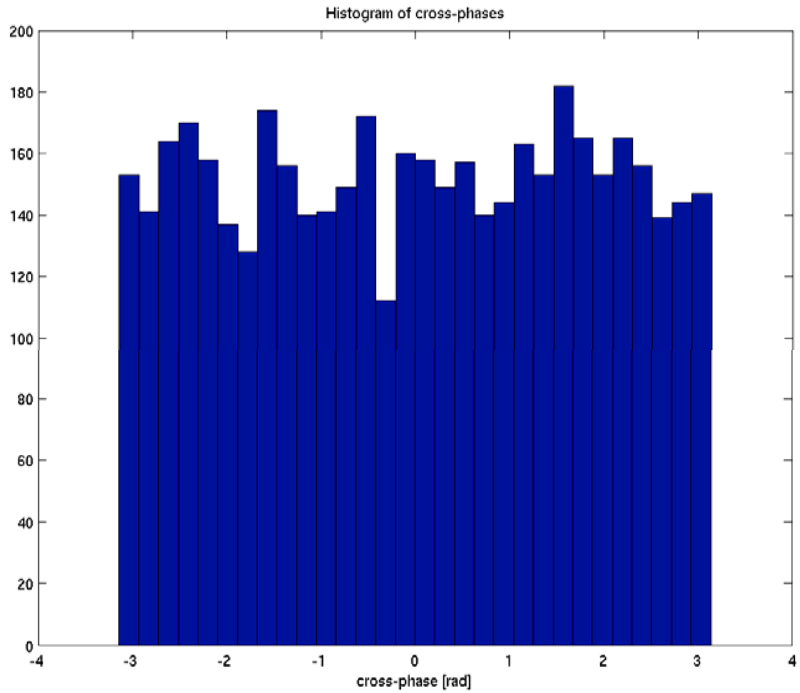

The cross-phase versus amplitude

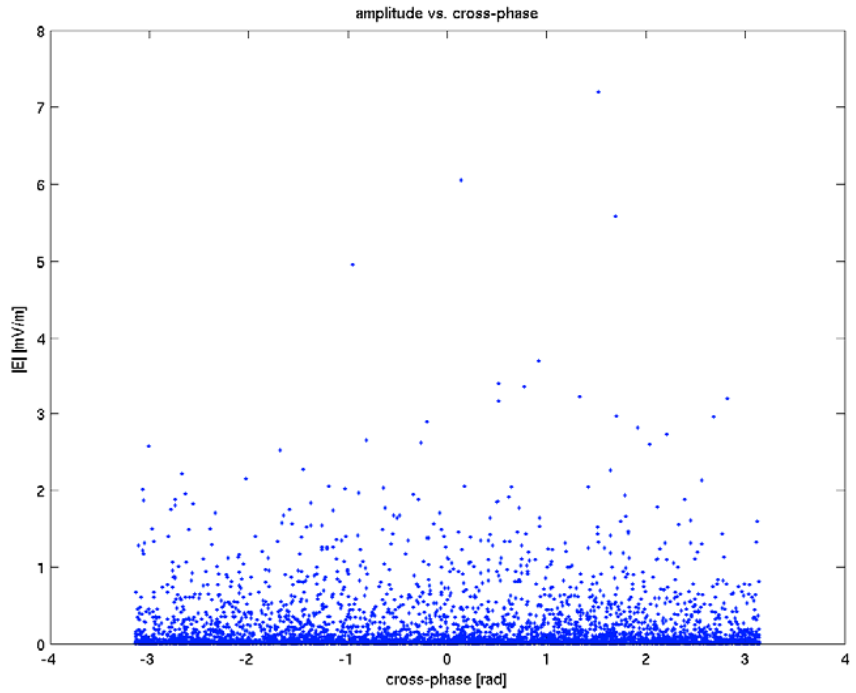

The cross-phases seem to be uniformly distributed with no apparent amplitude dependence.

Validity of the results, caveats

- The amplitude of the low-frequency waves is usually quite small, so may are not be well represented in the data 8-bit digital because of digitization error. However, the Fourier transform is known to be very robust in this respect, we included in the statistics only samples where the LF wave amplitude is high enough comparing to a digitization step.
- The weak low-frequency wave can be in principle generated by the non-linearity of the receiver. We checked our results against non-linear calibration of the WBD electronics and the observed waves seem to be stronger than the instrumental bias.

Probability distribution function of wave amplitudes

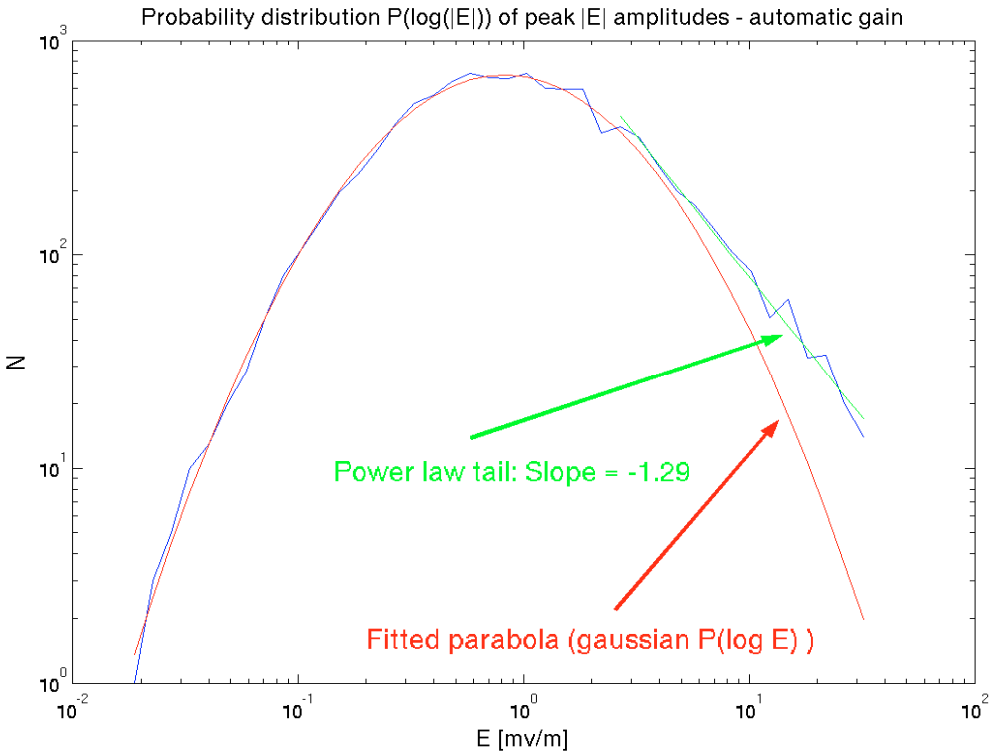

In this viewgraph is plotted the PDF of peak wave amplitudes P(log E)
in log-log axes (based on foreshock event from Feb 17, 2002). Apparently, the amplitudes are distrubuted according to a log-normal PDF with a power-law tail
at largest amplitudes. This suggests that the physics of large amplitude waves might be different from the physics at low amplitudes.

Properties of wave modulation

- From previous studies of foreshock waves (Bale et al, GRL, 1999), it is known that the characteristic modulation time of Langmuir waves is not independent of their amplitude as would be suggested by classical theory of parametric instabilities. The higher amplitude waves tend to have slower modulation than the low amplitude ones.

- Now we present a more quantitative study of the relationship between the modulation length and the amplitude based on WBD data.

How we estimate modulation time.

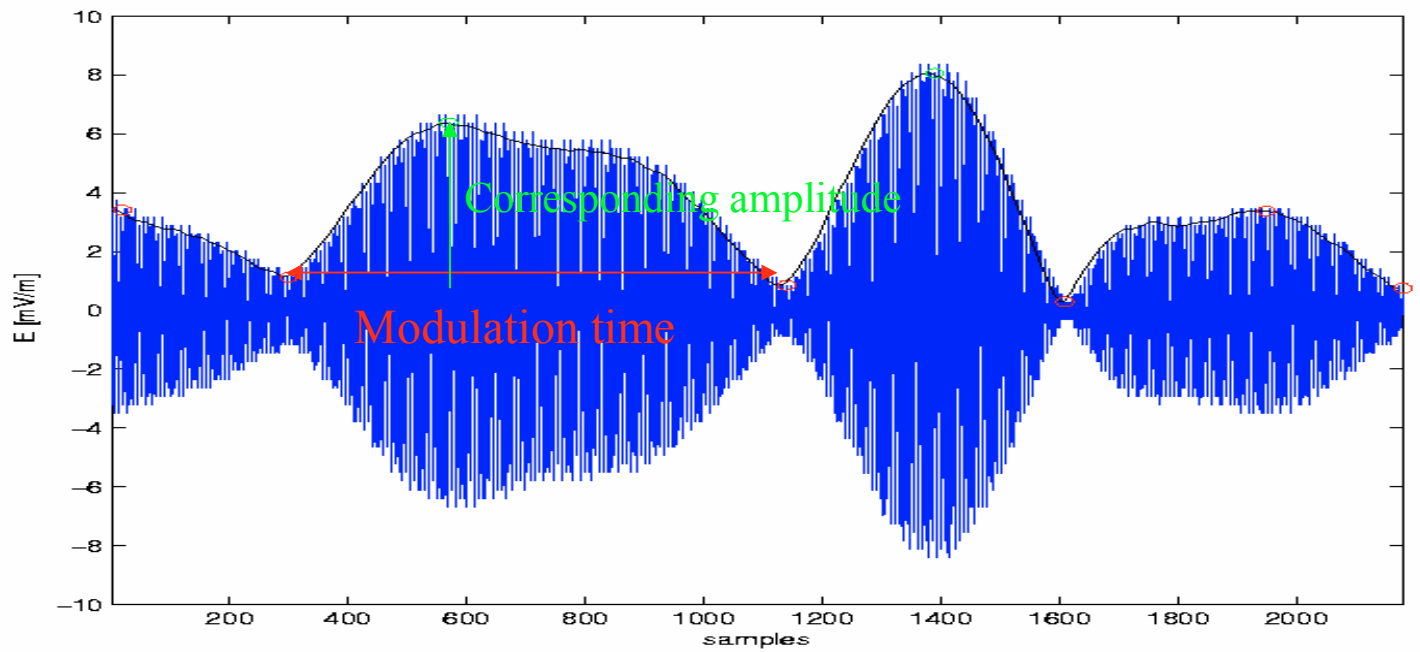

For our purposes, the characteristic modulation time is defined as the distance between two subsequent minima of the wave envelope. The corresponding peak amplitude is given by the field maximum in between.

Characteristic wave modulation time vs. wave amplitude.

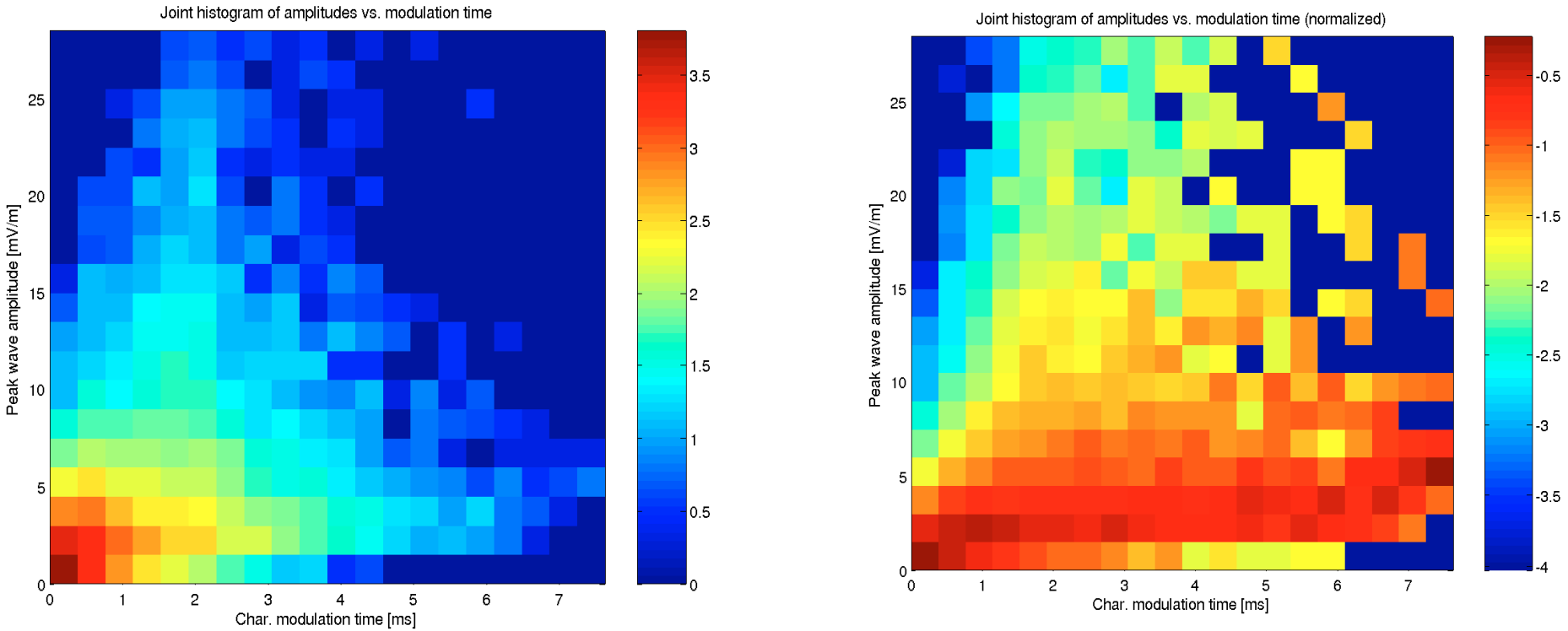

The left panel shows a 2D histogram of peak amplitudes (vert. axis) and char. modulation times (horiz. axis). The right panel shows the same histogram, now normalized to correct for smaller number of samples with large modulation times. The right plot clearly confirms the hypothesis of amplitude-scale dependence: the packets with longer modulation are likely to have larger amplitudes.

Conversion of modulation times to spatial scales

Now we will assume that the group velocity of Langmuir waves is negligible with respect to the solar wind flow velocity. Under this assumption we may consider the waves to be static structures convected by the solar wind over the satellite and convert the modulation time to spatial scales in the direction perpendicular to B (this direction is interesting for our interpretation) using the formula:

$$L = \Delta t * (\mathbf{n} \cdot \mathbf{V}) * \sin \alpha$$

Where **n** is the unit vector of antena orientation, **V** is the plasma flow velocity (from CIS), Δt is the modulation time and α is the angle between **n** and B.

Perpendicular modulation length vs. amplitude

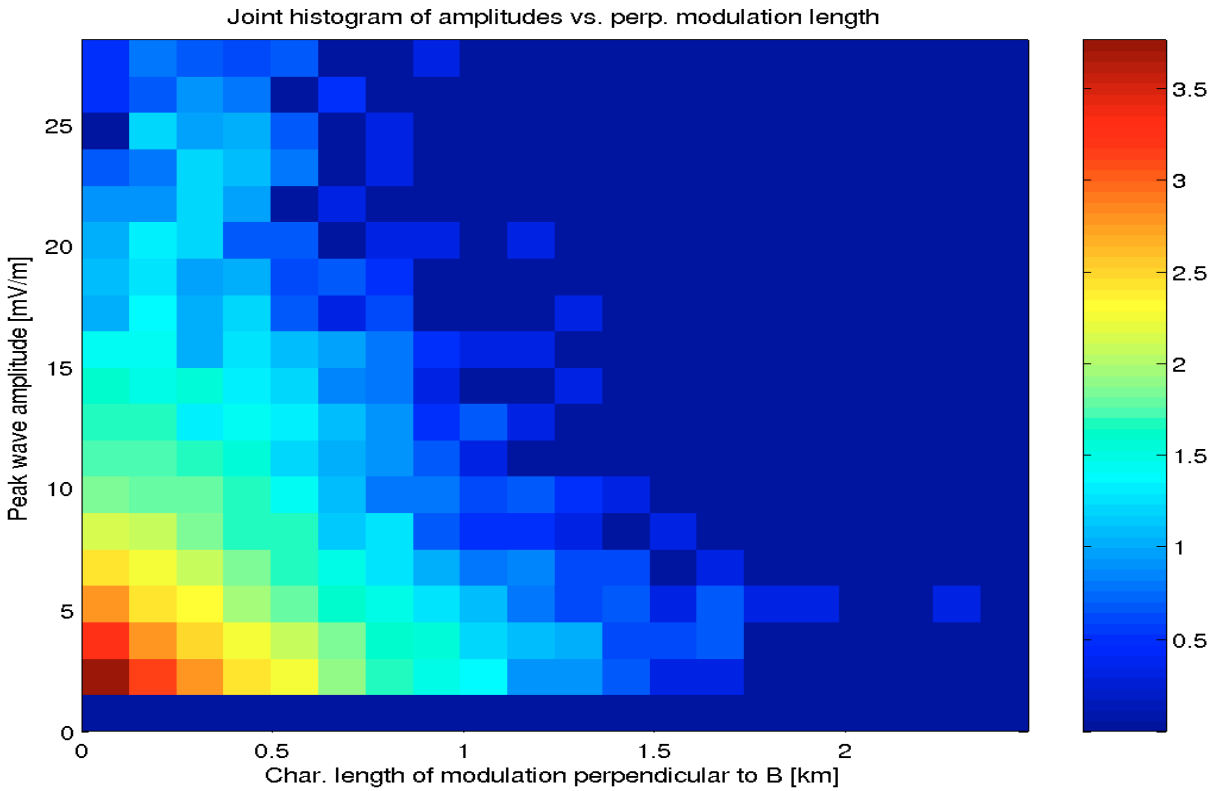

A histogram of peak amplitude versus the calculated modulation size in the direction perpendicular to B.

Numbers and estimates

$$T_e = 10eV, T_i = 20eV, n_e = 10cm^{-3}$$

$$\lambda_D(T_e + T_i) \sim 13m$$

$$d_e = \lambda_D(T_e) \sim 7.4m$$

$$\gamma_S \approx k\left(\frac{T_e}{M_i}\right)^{1/2}\left[\left(\frac{T_e}{T_i}\right)^{3/2}\exp\left[-\frac{1}{2}\left(\frac{T_e}{T_i}+3\right)\right]\right]$$

$$\omega_S^2 = \frac{\omega_{pi}^2}{1+1/k^2d_e^2}\left[1+3k^2d_i^2\left(1+\frac{1}{k^2d_e^2}\right)\right]$$

Nui

$$\omega_S^2 \approx k^2 \left(\frac{T_e + 3T_i}{M_i} \right)^{1/2}$$

$$\frac{\gamma_S}{\omega_S} \sim\approx \left(\frac{1}{2} \right)^{3/2} \exp\left(-\frac{7}{4} \right) = 6.1 * 10^{-2}$$

$$\sqrt{16\pi n(T_e + T_i)}\,(V/m) = 0.52(V/m)$$

Comparison of group velocities:

$$V_L = 3k_x d_e^2 \omega_p \sim 3\frac{V_{Te}}{V_b} V_{Te} \sin\theta$$

if beam has the energy $E_b = 1keV$

$$V_L \sim 0.3 V_{Te} \sin\theta \sim 4 \times 10^8 \sin\theta (cm/\sec)$$

$$V_S(cm/\sec) = c_S \sin\frac{\theta}{2} = \left(\frac{T_e + 3T_i}{M_i}\right)^{1/2} \sin\frac{\theta}{2} \approx$$

$$\approx 10^6\sqrt{30}\,\sin\frac{\theta}{2} = 0.55 * 10^5 \sin\frac{\theta}{2}(m/\sec)$$

$$V_L >> V_S$$

Threshold estimate:

$$\left(\frac{E_0^2}{16\pi n(T_e + T_i)}\right)^{1/2} > \frac{\pi}{4l}\sqrt{\frac{V_S V_L}{\omega_S \omega_p}}$$

$$E_0 > \frac{33000}{l}\sqrt{\sin\frac{\theta}{2}\sin\theta}(mV/m)$$

Electron-sound and Langmuir waves

$$\frac{\partial^2}{\partial t^2}\left(\Delta\phi - \frac{4\pi n_{h0} e^2}{T_h}\phi\right) +$$

$$+ \omega_{pc}^2\left(1 + \frac{3T_e}{T_h}\frac{n_{h0}}{n_0}\right) div\left[\frac{n_S}{n_0}\nabla\phi\right] +$$

$$+ \omega_{pc}^2\left(1 + \frac{3T_e}{T_h}\frac{n_{h0}}{n_0}\right)\Delta\phi - 3\omega_{pc}^2\lambda_{Dc}^2\Delta^2\phi = 0$$

$$\omega^2 = \frac{k^2 \lambda_{Dh}^2}{(k^2 \lambda_{Dh}^2 + 1)} \left[\omega_{ph}^2 \left(1 + \frac{3T_e}{T_h} \frac{n_{h0}}{n_0} \right) + 3\lambda_{Dc}^2 k^2 \right]$$

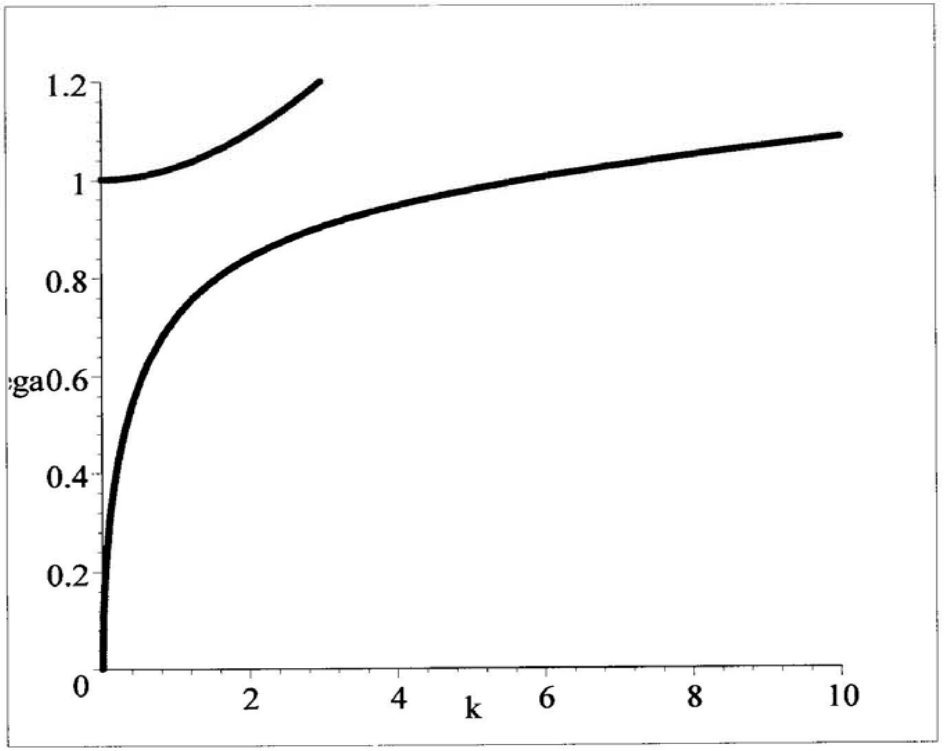

$$\left(\frac{\partial \Psi_0}{\partial t} - \Gamma_0 \Psi_0\right) = -i\frac{\omega_p}{2}\frac{\left(\vec{k_0},\vec{k_{eS}}\right)}{k_0^2}\frac{\rho_S}{n_c+n_h}\Psi_{eS}$$

$$\left[\frac{\partial}{\partial t} + \left(\gamma_{eS} + V_{eSx}\frac{\partial}{\partial x}\right)\right]\Psi_{eS} = -\frac{i\omega_p}{2}\frac{(\vec{k},\vec{k_0})}{k_0^2}\frac{\rho_S^*}{n_c+n_h}\Psi_0$$

$$\left[\frac{\partial}{\partial t} + \left(\gamma_S + S_x\frac{\partial}{\partial x}\right)\right]\rho_S = -i\omega_S\frac{\varepsilon_0\omega_p^2\left(\vec{k},\vec{k_0}\right)}{2\omega_{eS}\omega_L M_i C_S^2}\Psi_0\Psi_{eS}^*$$

$$\frac{|\ (\vec{k},\vec{E_0})\ |^2}{16\pi n_c M C_S^2 k^2} > \frac{\gamma_S \gamma_1}{\omega_S \omega_1}$$

$$\left[\ \frac{|\ (\vec{k},\vec{E_0})\ |^2}{16\pi n_c M C_S^2 k^2}\ \right]^{1/2} > \frac{\pi}{4l}\sqrt{\nu_3 \nu_2}\ .$$

$$E_0 > \sqrt{16\pi n_c M C_S^2}\ \frac{\pi}{4l}\sqrt{\frac{V_{gIS} V_{gES}}{\omega_{pc}\omega_S}}\ \frac{\sin\theta}{\cos\theta}$$

$$E_0 > 33000 mV/m \frac{\tan\theta}{l}$$

$$(\frac{\partial}{\partial t}+2\gamma_{ES})\int_0 |\ \mathbf{E}_{ES}(x)|^2 dx + 2v_{ESx}|\ \mathbf{E}_{ES}(L)|^2 =$$

$$=\mathrm{Im}\frac{\omega_p}{n_c+n_h}\int_0^L (\overrightarrow{E^*_{ES}}(x),\overrightarrow{E_0}(x))\rho^*_S(x)dx$$

$$\left(\frac{\partial}{\partial t}+2\gamma_S\right)\int_0^L |\ \rho_{IS}(x)|^2 - 2C_{ISx}|\ \rho_{IS}(0)|^2 =$$

$$= \frac{\varepsilon_0\omega_p^2}{2\omega_S\omega_{eS}(n_c+n_h)MC_S^2}\mathrm{Im}\int_0^L\left(\overrightarrow{E^*_{ES}}(x),\overrightarrow{E_0}(x)\right)\rho^*_{IS}(x)$$

Energy flux from the system through its borders is similar to lasers with imperfect mirrors

$$\frac{dW_2}{dt} = -V_{2x} \mid E_2 \mid_{x=0}^{2} - 2\gamma_2 W_2 + 2\int_0^l dx \,\mathrm{Re}(\alpha E_2 E_3^*)$$

$$\frac{dW_3}{dt} = -V_{3x} \mid E_2 \mid_{x=l}^{2} - 2\gamma_3 W_3 + 2\int_0^l dx \,\mathrm{Re}(\beta E_3 E_2^*)$$

Let us introduce the ratio:

$$\mu_2 = \frac{V_{2x} \mid E_2 \mid^2_{x=0}}{\int_0^l \mid E_2(x) \mid^2 dx} = \frac{V_{2x} \mid E_2 \mid^2_{x=0}}{W_2}$$

$$\mu_3 = \frac{V_{3x} \mid E_3 \mid^2_{x=l}}{\int_0^l \mid E_3(x) \mid^2 dx} = \frac{V_{3x} \mid E_3 \mid^2_{x=l}}{W_3}$$

$$\left(\frac{\partial \Psi_0}{\partial t} - \Gamma_0 \Psi_0\right) = -i\frac{\omega_p}{2}\frac{\left(\vec{k_0},\vec{k_{eS}}\right)}{k_0^2}\frac{\rho_S}{n_c+n_h}\Psi_{eS}$$

$$\left[\frac{\partial}{\partial t} + \left(\gamma_1 + \mu_{eS}\frac{V_{eS}}{L}\right)\right]\Psi_{eS} = -\frac{i\omega_p}{2}\frac{(\vec{k},\vec{k_0})}{k_0^2}\frac{\rho_S^*}{n_c+n_h}\Psi_0$$

$$\left[\frac{\partial}{\partial t} + \left(\gamma_S + \mu_S\frac{S_x}{L}\right)\right]\rho_S = -i\omega_S\frac{\varepsilon_0\omega_p^2\left(\vec{k},\vec{k_0}\right)\Psi_0\Psi_{eS}^*}{2\omega_{eS}\omega_L M_i C_S^2}$$

$$\frac{\varepsilon_0 |E_0|^2}{(n_c+n_h)M_i C_S^2} = \frac{16\omega_{eS}\omega_L\left(\gamma_S+\mu_S\frac{S_x}{L}\right)\left(\gamma_1+\mu_{eS}\frac{V_1}{L}\right)}{\omega_S\omega_p^3\frac{(\vec{k},\vec{k_0})^2}{k_0^4}}$$

SCALING LAW

$$\gamma_S >> \mu_S \frac{S_x}{l}$$

$$\gamma_1 << \mu_1 \frac{V_1}{l}$$

$$| \mathbf{E}_0 | \sim \sqrt{\gamma_S \mu_1 \frac{V_1}{l}} \sim \mathbf{I}^{-1/2}$$

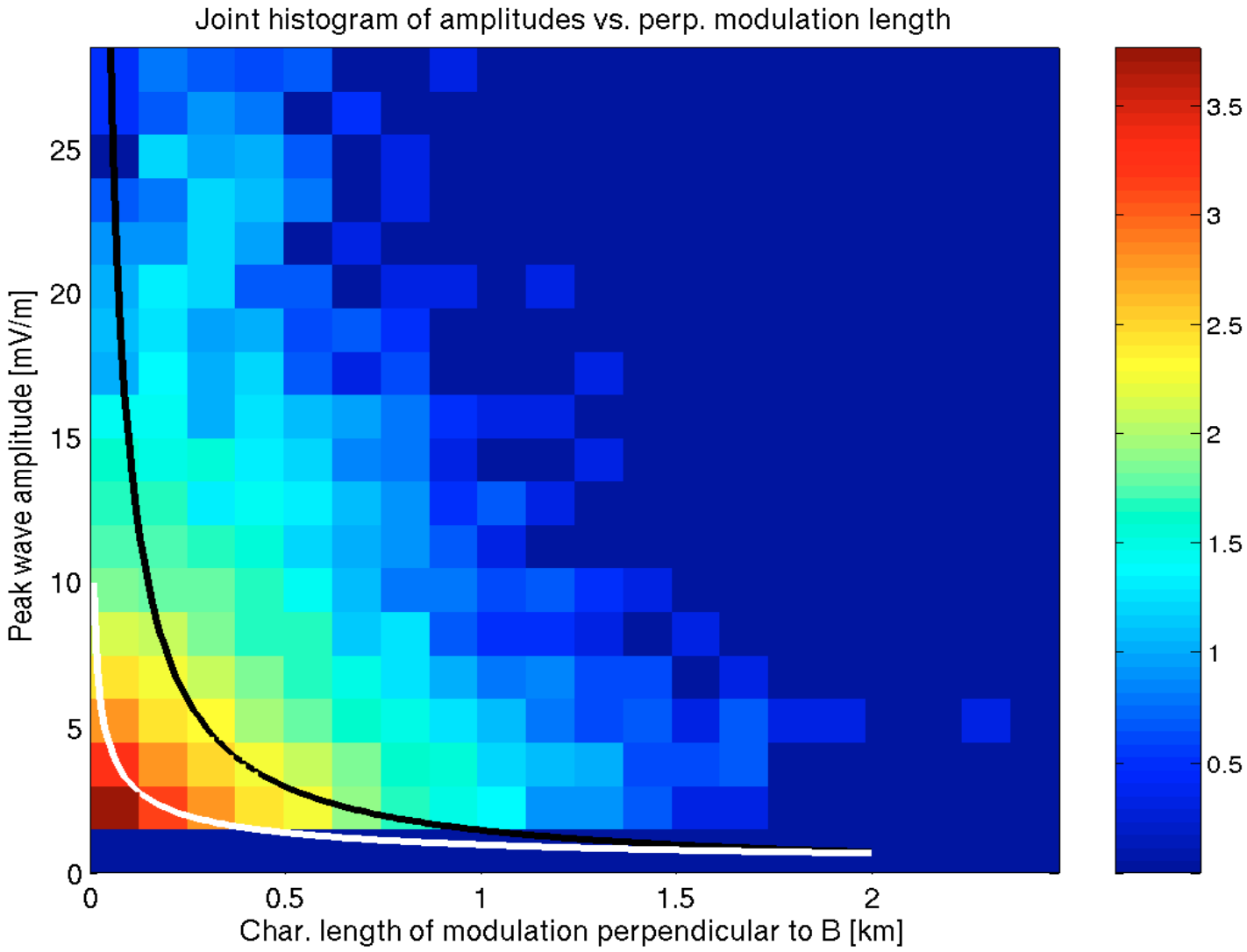
Joint histogram of amplitudes vs. perp. modulation length
Peak wave amplitude [mV/m]
0
5
10
15
20
25
0
0.5
1
1.5
2
Char. length of modulation perpendicular to B [km]
0.5
1
1.5
2
2.5
3
3.5

Conclusions

- We have shown, that the frequencies of the ion-sound waves in the foreshock are significantly correlated with the frequency separation of the two peaks in Langmuir wave spectrum.
- The correlation is especially good for higher amplitude waves
- These observations and analysis result in the conclusion that observed wave spectra can be interpreted as produced due to parametric instability